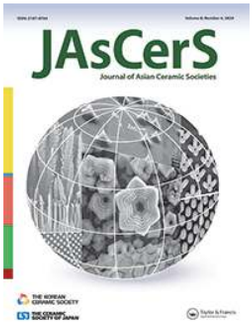

Journal of Asian Ceramic Societies

ISSN: (Print) (Online) Journal homepage: https://www.tandfonline.com/loi/tace20

Impact of forsterite addition on mechanical and biological properties of composites

Rajan Choudhary, Senthil Kumar Venkatraman, Inna Bulygina, Ankita Chatterjee, Jayanthi Abraham, Fedor Senatov, Sergey Kaloshkin, Artem Ilyasov, Maxim Abakumov, Marina Knyazeva, Dimitri Kukui, Frank Walther & Sasikumar Swamiappan

To cite this article: Rajan Choudhary, Senthil Kumar Venkatraman, Inna Bulygina, Ankita Chatterjee, Jayanthi Abraham, Fedor Senatov, Sergey Kaloshkin, Artem Ilyasov, Maxim Abakumov, Marina Knyazeva, Dimitri Kukui, Frank Walther & Sasikumar Swamiappan (2020) Impact of forsterite addition on mechanical and biological properties of composites, Journal of Asian Ceramic Societies, 8:4, 1051-1065, DOI: 10.1080/21870764.2020.1807695

To link to this article: https://doi.org/10.1080/21870764.2020.1807695

Published online: 24 Aug 2020.

JOURNAL OF ASIAN CERAMIC SOCIETIES
2020, VOL. 8, NO. 4, 1051–1065
https://doi.org/10.1080/21870764.2020.1807695

Impact of forsterite addition on mechanical and biological properties of composites

Rajan Choudhary[a], Senthil Kumar Venkatraman[b], Inna Bulygina[a], Ankita Chatterjee[c], Jayanthi Abraham[c], Fedor Senatov[a], Sergey Kaloshkin[a], Artem Ilyasov[a], Maxim Abakumov[a], Marina Knyazeva[d], Dimitri Kukui[d], Frank Walther[d] and Sasikumar Swamiappan[b]

[a]Center for Composite Materials, Laboratory "Biomedical Nanomaterials", National University of Science and Technology "Misis", Moscow, Russia; [b]Department of Chemistry, School of Advanced Sciences, Vellore Institute of Technology, Vellore, India; [c]Microbial Biotechnology Laboratory, School of Biosciences and Technology, Vellore Institute of Technology, Vellore, India; [d]Department of Materials Test Engineering, TU Dortmund University, Dortmund, Germany

ABSTRACT

The objective of designing a biocompatible and mechanically stable scaffold for hard tissue regeneration was achieved by fabricating diopside/forsterite composites. Superior mechanical strength, slow degradation, excellent antibacterial activity and good cell viability were attained with the increase in forsterite ratio in the composites whereas apatite deposition ability got enhanced as the diopside content was increased. The variation in the rate of apatite deposition on the surface of composites exhibited different surface topography such as nano-structured interconnected fibrous network and globular morphology. The scaffolds after one-month immersion in a physiological environment exhibited good Young's modulus and compressive strength. Clear and distinguishable prevention of bacterial growth confirms that composites have the potential to inhibit microbial colony formation of nine different clinical pathogens. The composite containing major diopside content was more effective toward *S. aureus* while the growth of *E. coli* was inhibited more by the composite containing a higher ratio of forsterite. The interaction of composites with MG-63 cells showed an enhancement in cell viability as the content of forsterite was increased. MTS assay confirmed the cytocompatibility of samples with negligible toxicity effects.

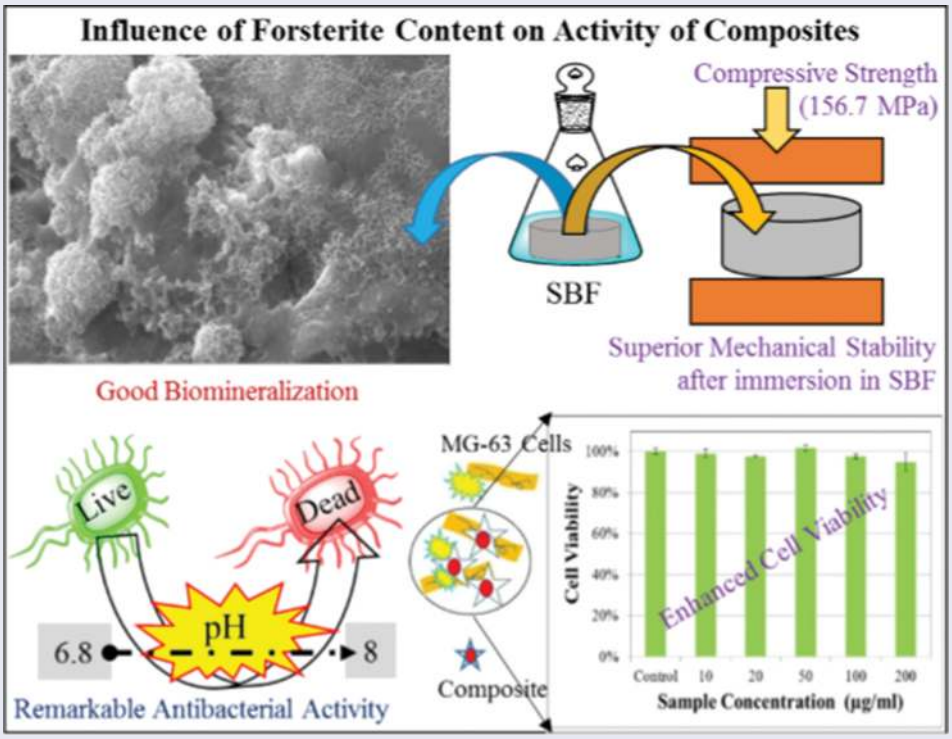

ARTICLE HISTORY
Received 16 March 2020
Accepted 5 August 2020

KEYWORDS
Magnesium Silicate Bioceramic; content-dependent; MTS assay; clinical pathogens; scanning electron microscopy

CONTACT Sasikumar Swamiappan ssasikumar@vit.ac.in Department of Chemistry, School of Advanced Sciences, Vellore Institute of Technology, Vellore, Tamil Nadu 632014, India

1. Introduction

Researchers are exploring the interaction between cells, tissue-stimulating signaling cues, and biomaterials to combat the diseases, injuries and defects related to bone [1]. Tissue engineering and regenerative medicine (TERM) are recognized as one of the most essential modules for surgical and medical practices in the twenty-first century [2]. Tissue engineering involves a combination of patient-derived cells with scaffolds having adequate biochemical and physicochemical properties that enable to develop a viable tissue or organ with clinical relevance for biomedical purposes [3]. The requirements of an ideal scaffold for hard tissue regeneration are biodegradability, bone inductive ability, mechanically stable and internal structure should facilitate cell proliferation and vascularization [4]. Thus, the concept of TERM has evolved as a potential approach to replace diseased/damaged body parts and avoid problems associated with immunological rejection, availability of donors and demand for compatible organs for transplantation [5,6].

Despite remarkable advancements in medical technology, currently, available bone substitutes lack proper degradation rate and insufficient mechanical strength for long term applications [7]. The faster degradation causes loosening of the implant and therefore the rate of resorption should match with the rate of tissue regeneration. The mismatching of mechanical properties between the surrounding tissue and implant either fails to provide sufficient structural support to the regenerating tissues during degradation and remodeling or leads to stress shielding at the implant site [8]. The concept of composites has indicated to achieve superior biochemical and mechanical properties over individual components. Bone is a well-known apatite-collagen natural composite material that serves as a platform for developing new materials [9]. Attempts are made to fabricate scaffolds that could initiate tissue regeneration through bioactive fixation. An earlier finding suggested that the excellent biological and mechanical properties of bioceramics containing $CaO.MgO.SiO_2$ groups are considered as promising candidates for hard tissue regeneration when compared to hydroxyapatite [10].

Diopside is the first magnesium-based silicate ceramic which showed bioactivity [11]. Diopside is a chain-silicate mineral which comprises of covalently bonded silica network, interrupted and modified by Mg^{2+} and Ca^{2+} ions. Literature suggests that the dissolution of Ca, Mg and Si ions from diopside plays a key role in cell proliferation and differentiation [12]. Amongst all ternary CaO-MgO-SiO_2 ceramic materials, the diopside possesses slower degradability, improved mechanical property and good cytocompatibility [13,14]. Previously diopside was incorporated in the different ceramic matrix (alumina, HAp, forsterite) for preparing composites. These results indicate that an increase in diopside content in the composite improves the reactivity of these composites in the physiological environment [15–17].

Forsterite (Mg_2SiO_4) is a dimagnesium silicate with superior mechanical properties over calcium phosphates and calcium magnesium silicates. In addition, forsterite is a biocompatible material that possesses HAp deposition ability and stimulates proliferation and adhesion of osteoblasts [10]. The influence of forsterite content on the mechanical properties and apatite formation ability of bioglass/forsterite composites was studied [18]. It was also observed that an increase in forsterite content in the composite plays a key role in enhancing mechanical strength as well as apatite deposition on the surface of the composites. Later, Sebdani and Fathi (2012) coated HAp/bioglass/forsterite composites on 316 L stainless steel implant. An increase in apatite deposition with the increase in forsterite concentration indicates that it can be used as a potential bioceramic in hard tissue regeneration [19].

The bacterial adhesion on biomaterial surfaces results in the destruction of bones as well as joints [20]. Prevention of bacterial infections is considered as the major concern in the biomedical field. Earlier findings suggest that bioactive glass possesses reasonable antibacterial activity [21–23]. Hence, different metal ions (silver, copper or zinc) were doped in HAp to examine its bactericidal properties [24]. Studies reveal that the accretion of these metallic ions causes cytotoxicity in bone by affecting its biocompatibility [25]. These issues can be overcome by designing a suitable biomaterial with antibacterial properties and biocompatibility. Saqaei et al. (2016) observed significant improvement in antibacterial activity of 58S bioactive glass after fabricating its composites with forsterite [26]. Certain parameters such as the particle size, surface area, concentration, pH of the medium and exposure time affect the antibacterial activity of the silicate bioceramics [27–29].

The present study is aimed toward designing a biocompatible, degradable, mechanically strong scaffold with antibacterial activity for biomedical applications. Authors also confirm that for the first time simple method (powder mixing and pelletizing) was employed to fabricate diopside/forsterite scaffolds to study the effect of compositional ratio and chemical constituent on biomineralization, dissolution, degradation, mechanical properties, antibacterial activity and cellular behavior.

2. Experimental procedure

2.1. Materials and methods

Glycine (99.5%, AR, SDFCL), Eggshell Powder, Tetraethyl Ortho Silicate (TEOS) (98%, Acros Organics), Magnesium Nitrate (99.0%, LR, SDFCL), Concentrated Nitric Acid (69–-72%, LR, SDFCL), Sodium Chloride AR (99.9%, SDFCL), Sodium Bicarbonate AR (99%, SDFCL), Potassium

Chloride AR (99.5%, SDFCL), Di-potassium Hydrogen Orthophosphate AR (99.0%, SDFCL), Magnesium Chloride AR (99.0%, SDFCL), Conc. Hydrochloric Acid LR (35–38%, SDFCL), Calcium Chloride AR (98%, SDFCL), Sodium Sulfate Anhydrous AR (99.5%, SDFCL), Tris(hydroxymethyl)aminomethane AR (99.8%, SDFCL) and Deionized water. All the materials were used as such without any further purification.

2.2. Preparation of bioceramics and their composites

The diopside and forsterite powders were prepared by the sol-gel combustion method using glycine as fuel as mentioned elsewhere [27,28]. Briefly, the stoichiometric oxidant/fuel ratio was used for the synthesis of diopside and forsterite. An equal molar concentration of calcium nitrate derived from eggshell powder and magnesium nitrate solution was mixed in a beaker for the preparation of diopside. Glycine solution was added into the beaker and stirred constantly to obtain a complex mixture of starting reagents. Finally, TEOS (Tetraethyl Ortho Silicate) was poured into the beaker and concentrated nitric acid was added dropwise to adjust the pH of the reaction solution to 1.7. The resultant solution was stirred by using a magnetic stirrer leading to the formation of the gel in a beaker. The gel was aged for about a week and the volatile moiety, moisture was eliminated by drying at 150 °C. The dried powder was combusted in a preheated muffle furnace at 400 °C for half an hour. The decomposed precursor was calcined at 1100 °C.

Stock solutions of glycine and magnesium nitrate were prepared by dissolving in double-distilled water for the synthesis of forsterite. Magnesium nitrate and glycine were mixed in a beaker at room temperature under stirring conditions leading to the formation of the metal complex. To this reaction mixture, TEOS was added. The pH of the reaction solution was adjusted to 1.7 by the drop-wise addition of conc. nitric acid. The resultant reaction mixture was stirred vigorously for the homogeneous mixing of the starting materials. This step initiates the hydrolysis of TEOS leading to polycondensation and finally the formation of the polymeric gel-like network. Later, the gel was aged for about four days and dried at 70 °C in a hot air oven. The dried powder was decomposed in a preheated muffle furnace at 400 °C for 30 min. The combusted precursor was grinded into a fine powder and calcined at 900 °C to achieve purity. The phase purity of diopside and forsterite powders was confirmed by XRD, functional groups were determined by FT-IR Spectroscopy and surface morphology was studied by Scanning Electron Microscopy.

The pure diopside and forsterite powders were utilized to fabricate their composites. The composites were prepared manually by grinding diopside with forsterite in different compositional ratios (Table 1) with the help of mortar and pestle. The resultant mixture was pelletized into circular scaffolds (13 mm × 2 mm) by using hydraulic KBr pellet press under a pressure of 20 MPa. The scaffolds were removed carefully from the pellet press and dried at 150 °C to remove the atmospheric moisture. The dried scaffolds were placed separately in the conical flasks containing SBF solution (50 ml) and incubated at 37 °C ± 0.3. The SBF solution was changed after every 24 h in order to provide an uninterrupted supply of essential ions responsible for apatite precipitation. After every 7 days, the samples were removed from the SBF, washed with double distilled water and dried at 80 °C in hot air oven prior to the surface analysis by XRD, FT-IR and SEM/EDX.

Table 1. Composition of diopside/forsterite composites.

S. No	Code	Composition of Diopside (wt. %)	Composition of Forsterite (wt. %)
1	DF1	75	25
2	DF2	50	50
3	DF3	25	75

2.3. In vitro experiments

2.3.1. Biomineralization assay

The bioactivity of the diopside/forsterite composites was analyzed by immersing them in the simulated body fluid (SBF). Simulated body fluid has a similar ionic concentration and composition to that of human blood plasma. It was prepared in a single batch by dissolving the required chemicals of analytical grade in the sequence as per Kokubo and Takadama protocol [30]. The appropriate quantities of reagents for the preparation of SBF were dissolved in double distilled water with constant stirring at room temperature as shown in Table 2. The pH of simulated body fluid was adjusted to 7.40 ± 0.2 by using 1 M HCl.

2.3.2. Dissolution study

The as-prepared fresh SBF and SBF collected after every 7th day was stored at −10 °C in the refrigerator to study the ionic concentration by inductively coupled plasma-optical emission spectroscopy.

2.3.3. Degradation analysis

The degradation behavior of diopside/forsterite composites was studied by observing the weight change of the composites before and after immersion in the SBF medium for 30 days. Different ratios of pure diopside and

Table 2. Chemical Composition of SBF Solution (1 Liter).

Order	Reagent	Amount
1.	NaCl	8.035 g
2.	$NaHCO_3$	0.355 g
3.	KCl	0.225 g
4.	$K_2HPO_4 \cdot 3H2O$	0.231 g
5.	$MgCl_2 \cdot 6H2O$	0.311 g
6.	1.0 M HCl	39 mL
7.	$CaCl_2$	0.292 g
8.	Na_2SO_4	0.072 g
9.	Tris(hydroxymethyl)aminomethane	6.118 g

forsterite were finely grounded and molded into cylindrical scaffolds (13 mm diameter × 6.5 mm height) at 20 MPa by the hydraulic press and heated thermally at 1300 °C at a rate of 5 °C/min for 3 h. The samples were cooled to room temperature. The initial weights of the samples were measured using a weighing balance and then immersed in SBF (static condition) at 37 °C ± 0.3. After 30 days, the scaffolds were taken out from SBF, dried at 150 °C for 24 hours and the degradation process was monitored gravimetrically by the change in weight. The test was repeated three times for each composite and the data were given as a mean with the standard deviation. The weight loss from the scaffolds was expressed in percentage (%).

2.3.4. Mechanical testing

The procedure followed for the preparation of diopside/forsterite scaffolds for mechanical studies was as per ASTM specifications discussed elsewhere [14]. Briefly, different ratios of pure diopside and forsterite powders were finely grounded and molded into cylindrical scaffolds (13 mm diameter × 6.5 mm height) at 20 MPa by the hydraulic press and heated thermally at 1300 °C at a rate of 5 °C/min for 3 h. The diopside/forsterite composites obtained after degradation studies were examined for mechanical stability by using the universal testing machine (UTM) INSTRON 8801 with a load weight accuracy of ± 0.5%. The composites were tested at an extension rate of 0.6 mm/min and a compression rate of 1 mm/min. The test was repeated three times for each composite and the data were given as a mean with the standard deviation.

2.3.5. Antibacterial activity

Broth dilution technique was adopted to examine the antibacterial activity of composites against nine clinical bacteria's (*Staphylococcus aureus, Enterococcus species, Escherichia coli, Serratia marcescens, Pseudomonas aeruginosa, Klebsiella pneumoniae, Salmonella species, Shigella species*, and *Proteus mirabilis*). The pathogenic bacterial strains were suspended in Luria-Bertani broth in the presence of different concentrations (0.5, 1 and 2 mg/ml) of composites [31]. The broth containing the pathogens and composites was incubated under shaking conditions for 24 h and the bacterial growth was determined by observing the optical density by ELISA (Enzyme-Linked Immunosorbent Assay) reader at 600 nm (Biotek-*elx*800). Bacterial growth without composites was used as a control sample and compared with the composites containing bacterial suspension to evaluate the percentage of inhibition [32]. The dilutions of control and test samples were plated on Mueller-Hinton agar plates to observe the formation of colonies before and after the treatment with composites. The change in pH of the culture medium during the incubation period was analyzed to study its influence on the bacterial inhibition by the composites. The antibacterial study of the composites was conducted in triplicates (n = 3) and thus the results obtained from the test were represented as a mean with standard deviation. Well diffusion technique was also conducted to study the antibacterial study of the composites, however, the lower diffusion capacity of the composites in agar medium did not show any convincing results which could be confirmed to be the antibacterial effect of the composites.

The activity of the composite particles on the bacterial isolates was studied under the scanning electron microscope. The samples were washed thoroughly with ethanol for 10 min in 70%, 10 min in 95%, and 20 min in 100% continuously and air-dried. The air-dried samples were then coated with gold in sputter coater which prevents the sample from getting charged. The samples were then analyzed in SEM under a high vacuum at 10 kV [33,34].

2.3.6. MTS assay

The samples were sterilized in an autoclave at 121°C for 1 hour prior to cellular studies. MG-63 osteosarcoma cell culture was grown on cell medium DMEM/F12 (Dulbecco's Modified Eagle Medium: Nutrient Mixture F-12) with 10% FBS (Fetal Bovine Serum) and 1% L-glutamine in an incubator at a temperature 37°C and 5% CO_2 concentration. The CellTiter 96® AQueous One Solution Cell Proliferation Assay by Promega Corp. (USA), contained a tetrazolium compound (MTT), was used for determining the number of viable cells in proliferation.

MG-63 culture cells were plated in a 96-well plate in an amount of 15 thousand/well in volume 100 µl/well. Samples for the MTS assay were weighed into Eppendorf in an amount of 20 mg/ml. Then a suspension of these particles was obtained in PBS. A suspension of particles was instilled into the wells of a 96-well plate with pre-seeded cells so that the final concentration of particles was 200 µg/ml, 100 µg/ml, 50 µg/ml, 20 µg/ml, 10 µg/ml of medium. Each well had three repetitions. Cells were incubated with samples for 48 hours. After this, CellTiter 96® AQueous One Solution Cell Proliferation Reagent was added to wells in an amount 20 µl/well for 4 hours. Further, part of the medium (without particle) was taken into a new clean 96-well plate for measuring optical density. The optical density data were recorded at a wavelength of 490 nm on spectrophotometer Multiskan GO (Thermo Scientific, USA). As a control, cells were used to which no powders were added. Cell viability levels were calculated using the following formula:

The standard deviation (SD) was calculated for 6 replicates. Dunnett's multiple comparison test was used with significance $P < 0.05$.

3. Characterization

Powder X-Ray Diffractometer (Bruker, D8 advance, Germany), using Cu Kα, Ni-filtered radiation was used

for phase identification of the samples after immersion in SBF. The maximum angular accuracy allowed for 2θ deviation is ± 0.010. Functional groups present in composites were examined by FT-IR spectroscopy (IR Affinity-1, Shimadzu FT-IR spectrophotometer) using KBr method. The FT-IR spectrum was recorded from 4000 cm^{-1} to 400 cm^{-1} regions with 4 cm^{-1} resolution. Scanning electron microscopy (SEM-CARL ZEISS and TESCAN MIRA) were used to analyze the surface morphology and Energy-dispersive X-ray spectroscopy (EDX- OXFORD Inc. and EDAX Ametek Inc.) were used to study the elemental composition of the diopside/ forsterite composites. Inductively coupled plasma-optical emission spectroscopy (PerkinElmer, ICP-OES Optima 5,300 DV) was used to determine the ionic concentration of fresh SBF and SBF collected after apatite deposition. The SBF was not diluted before ICP analysis since 50 ml of SBF was used. The instrument was calibrated with a standard solution for each ion analysis. The wavelength used for different ions is as Ca – 317.933 nm, Mg – 285.213 nm, P – 213.617 nm and Si – 251.611 nm. Scanning electron microscopy (SEM-CARL ZEISS) and Energy-dispersive X-ray spectroscopy (EDX-OXFORD Inc.) was used to analyze the microstructure and elemental composition of the composites after immersion in SBF. Before SEM characterization, the composite scaffolds (DF1, DF2, DF3) were dried at hot air oven and then mounted on the stubs with adhesive carbon tapes. The composites were coated with gold in a sputter coater. The samples were analyzed under a high vacuum at 10 kV.

4. Results and discussion

4.1. Characterization of diopside and forsterite

4.1.1. Functional group and XRD analysis

FT-IR spectrum of the calcined product reveals the characteristic functional groups associated with the diopside (Figure 1(a)). The O-Ca-O non-bridging bending (nbr) vibrational modes were observed at 412 cm^{-1} and O-Mg-O non-bridging bending vibrational modes at 455 to 503 cm^{-1} respectively. The O-Si-O bending mode was observed at 634 and 671 cm^{-1} and the bands at 864 and 960 cm^{-1} are associated with Si-O symmetric stretching. The Si-O-Si symmetric stretching was found at 1066 cm^{-1}. FT-IR spectrum of calcined forsterite (Figure 1(b)) indicates the presence of all fundamental groups associated with forsterite. The band in the range of 470 cm^{-1} is attributed to modes of octahedral MgO_6. The peaks appearing in the range of 505 and 613 cm^{-1} are associated with SiO_4 bending vibrations. The stretching modes of SiO_4 bond were observed from 842 to 1006 cm^{-1}, respectively.

The XRD pattern (Figure 1(c)) of the diopside prepared by the sol-gel combustion method was

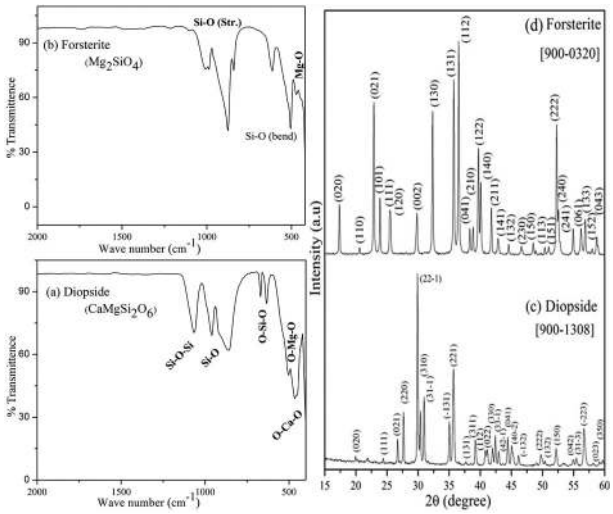

Figure 1. FT-IR spectra and indexed XRD pattern of diopside and forsterite.

matched and indexed as per standard JCPDS data card no. 900–1308. The crystal system of the diopside is monoclinic. The XRD pattern of forsterite (Figure 1(d)) was matched with the standard JCPDS card no. 900–0320 and indexed. The crystal system of forsterite was found to be orthorhombic.

4.1.2. Surface and elemental analysis

The particle analysis by means of SEM presents a size distribution of diopside bioceramics from sub-micrometer up to micrometer (Figure 2(a)). The size of forsterite particles is less than 1 micrometer and has homogeneous distribution (Figure 2 (b)). The EDX spectra (Figure 2(c, d)) shows the chemical composition of investigated bioceramics.

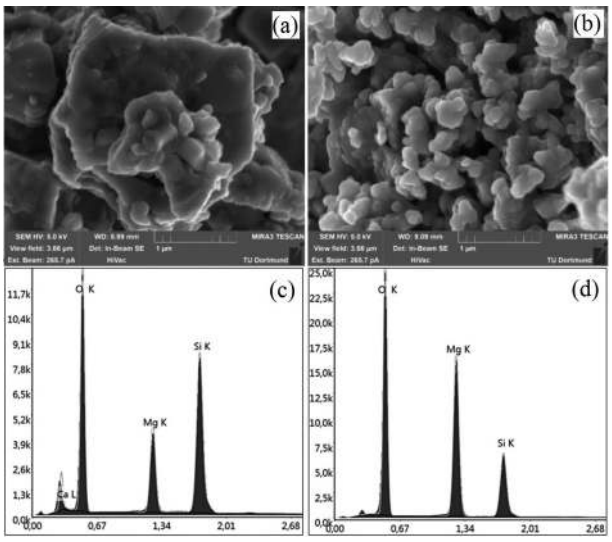

Figure 2. SEM/EDX spectra of diopside: $CaMgSi_2O_6$ (a, c) and forsterite: Mg_2SiO_4 (b, d).

4.2. Characterization of composites

4.2.1. XRD analysis of composites

The presence of diopside and forsterite phases in composites was analyzed by powder-XRD (Figure 3). The existence of characteristic peaks associated with pure diopside and forsterite phases was found in all the composites. The broadening of diopside and forsterite highest intense peak was noticed after the preparation of composites. The variation in the compositional ratio of diopside and forsterite in the composites was also observed in the XRD patterns. The XRD pattern of DF1 composite (Figure 3(a)) revealed the dominance of the diopside phase over forsterite whereas in the case of DF3 composite (Figure 3(c)) the forsterite was found to the major phase and diopside as a minor phase. Moreover, the DF2 composite (Figure 3(b)) has shown the presence of balanced diopside and forsterite phases as it contained an equal amount of diopside and forsterite. Thus, an increase in forsterite content in the composites resulted in an increase in the intensity of its characteristic peaks and vice versa. This observation confirmed the preparation of diopside/forsterite composites.

4.2.2. Surface and elemental analysis of composites

The SEM analysis of diopside/forsterite composites reveals similar surface morphology and particle size distribution (Figure 4). The EDX spectra indicate a higher amount of magnesium in chemical composition proportionally to a higher ratio of forsterite in the composites (Table 3).

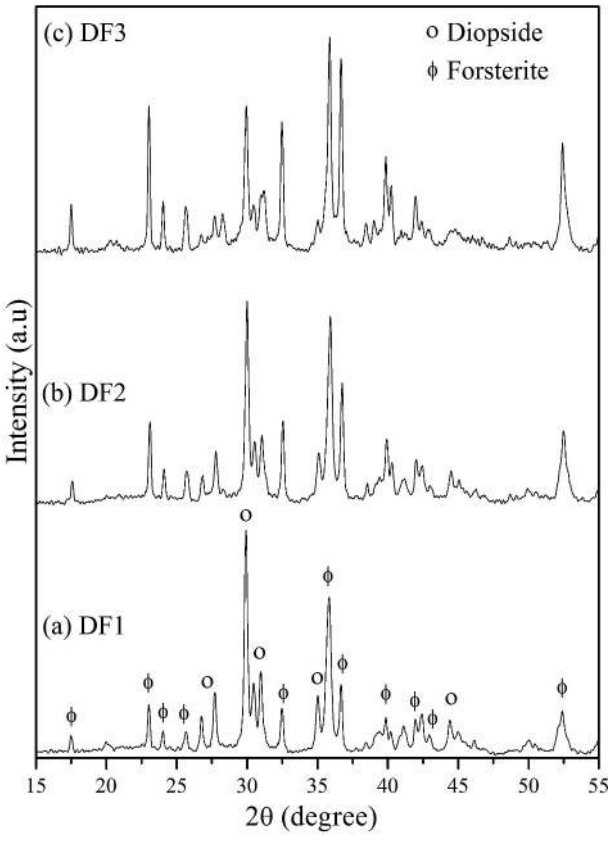

Figure 3. XRD pattern of composites.

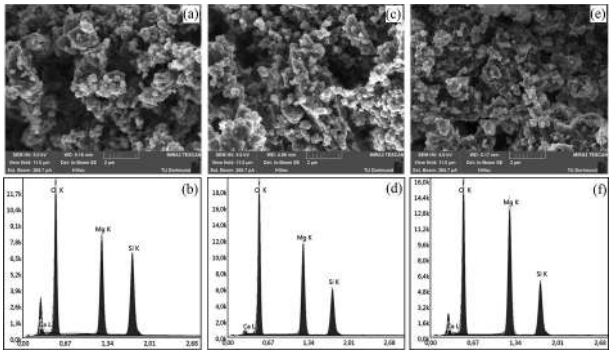

Figure 4. SEM/EDX spectra of diopside ($CaMgSi_2O_6$)/Forsterite (Mg_2SiO_4) composites (DF1- a, b; DF2- c, d; DF3- e, f).

4.3. Mechanism of apatite deposition on the surface of diopside/forsterite composites

The diopside/forsterite composites undergo a series of interfacial reactions after soaking in SBF. Initially, alkaline earth cations (Ca^{2+} and Mg^{2+}) from the composites were exchanged with the hydrogen ions present in the SBF. This results in the breakdown of the silica network into silanol (Si-OH) at the composite-SBF interface. Further, silanol undergoes a polycondensation reaction with hydroxyl ions (OH^-) from the SBF to form a silica-rich layer (Si-O^-) with the elimination of water. This layer is responsible for offering necessary sites to induce apatite nucleation. The negatively charged silica-rich layer attracts cations (Ca^{2+}) from the SBF and later anions (PO_4^{2-}) initiate apatite formation at the interface. The consumption of calcium and phosphorus ions during Ca-P deposition leads to a reduction in their concentration in SBF. This step proceeds continuously until an amorphous $CaO\text{-}P_2O_5$ film is deposited over the surface. Finally, carbonate and hydroxyl anions present in the SBF crystallize the film into calcium deficient hydroxycarbonate apatite (HCA) [35].

Table 3. Chemical composition of diopside/forsterite composites investigated by quantitative EDX analysis.

Composite Samples	Element	wt.%
DF1	O K	38.67
	MgK	21.98
	SiK	23.06
	CaK	16.29
DF2	O K	43.75
	MgK	30.46
	SiK	19.42
	CaK	6.39
DF3	O K	38.25
	MgK	37.58
	SiK	20.31
	CaK	3.85

4.4. Biomineralization studies

4.4.1. Dissolution analysis of composites during immersion in SBF

The calcium ion concentration in the SBF was observed to be low because the weight measurement of calcium chloride was affected due to its hygroscopic and deliquescent nature. Moreover, the assay percentage (98%) of calcium chloride, standard errors of the instruments used (weighing balance, ICP-OES), and occurrence of human error during the analysis of the samples might have influenced the concentration of calcium ion in the SBF. The dissolution behavior of diopside/forsterite composites was studied to understand their performance in the SBF solution (Figure 5). The DF1 composite shows a decrease in the concentration of Ca and P ions in the SBF throughout the study whereas the concentration of Mg and Si ions was found to increase in the first week and then decreases gradually (Figure 5(a)). When scaffolds are immersed in SBF, the cations (Ca^{2+}, Mg^{2+}) are exchanged with hydrogen ions due to the dissolution and diffusion process. The release of these cations into the SBF and attack of H^+ ion on the composite surface causes the breakdown of the silica network, thereby causing slight leaching of Si ion into the SBF. Among all these ions, Ca and P are required for apatite deposition. The DF1 composite shows constant consumption of Ca and P ions from the SBF medium revealing its ability to deposit hydroxyapatite. The formation of the apatite layer might have covered the major portions of the DF1 composite surface. Hence, the release of Si ion into the SBF got controlled after 7 days as the Si layer was covered with HAp.

The dissolution behavior of DF2 composite was found to be slower than that of DF1 in terms of the consumption of Ca and P ions from the SBF (Figure 5 (b)). The major reason for the difference in dissolution behavior was due to the leaching of Mg ion in the SBF in higher concentration. This might have restricted the utilization of calcium ion from the SBF. It has been reported that the release of magnesium at higher concentration in the physiological medium hinders the biomineralization ability of bioceramics [36]. These factors have delayed the apatite deposition on the surface of the DF2 composite.

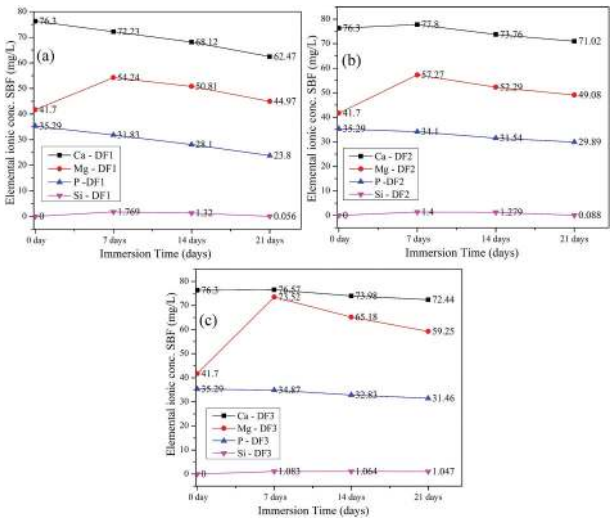

Figure 5. Dissolution study of composites during immersion in SBF: DF1 (a), DF2 (b) and DF3 (c).

DF3 composite indicates a sharp rise in the concentration of magnesium ion (Figure 5(c)) when compared to the other two composites. This may be due to the increase in the concentration of forsterite in the DF3 composite. The negligible consumption of calcium and phosphorus ions from the SBF resulted in poor apatite formation activity of the DF3 composite.

Ni et al. (2008) concluded that the change in Ca/Mg ratio directly affected the biomineralization activity of wollastonite/forsterite composites [37]. Hence, a decrease in the consumption of Ca and P ions was noticed as the content of forsterite in the composite was increased up to 70%. Vallet-Regi et al. (1999) emphasized that the rate of apatite formation is affected by the increasing magnesium content in the bioceramics [36]. Moreover, magnesium ion delayed the crystallization rate of amorphous Ca-P film and impeded the conversion of amorphous $CaO\text{-}P_2O_5$ into stable apatite. These could be the major factor responsible for the delayed HAp deposition on the surface of the DF3 composite.

4.4.2. FT-IR analysis of deposited apatite

The surface of diopside/forsterite composites after bioactivity studies was characterized by FT-IR spectroscopy to examine the absorption bands of different functional groups associated with the apatite structure. The FT-IR spectra (curve a in Figure 6) of DF1 after immersion in SBF shows bending vibration modes of phosphate groups at 459, 505 and 613 cm^{-1} while stretching vibration bands of phosphate in the range of 960, 981 and 1058 cm^{-1}. A similar FT-IR spectra was observed for DF2 (curve b of Figure 6). The sharp peaks at 466, 503 and 611 cm^{-1} correspond to the bending vibration of the phosphate group. The triplets in the range of 960, 983 and 1058 cm^{-1} represent stretching vibrations of the phosphate group. The IR spectra of DF3 composite (curve c of Figure 6) shows the appearance of peaks attributed to bending vibrational modes of phosphate at 451, 503 and 611 cm^{-1}. The dual peaks at 960 and 1064 cm^{-1} represent O-P-O stretching vibrations.

When a scaffold was immersed in the SBF, cations (Ca^{2+}, Mg^{2+}) of the composites were replaced by hydrogen ion and the breakdown of Si-O-Si groups formed Si-OH at the reactive interface. These groups further undergo a polycondensation reaction with OH^- ions and lead to the silica-rich layer formation. This layer provides necessary sites for apatite deposition

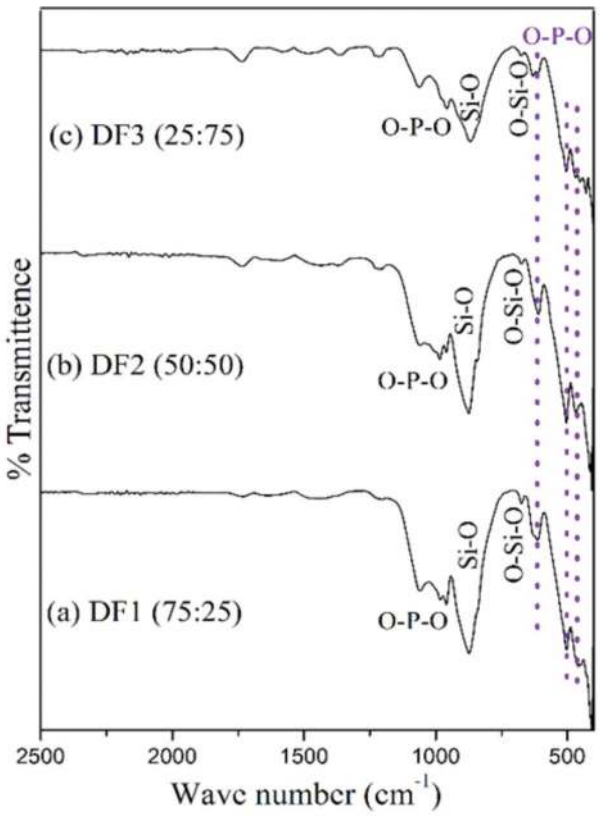

Figure 6. FT-IR spectra of diopside/forsterite composites after immersion in SBF.

[38]. These reactions cause replacement of O-Mg-O, O-Ca-O and Si-O-Si groups by phosphates during HAp formation.

4.4.3. XRD analysis of deposited apatite

When the surface of all three composites was examined by powder XRD after a week of immersion, apatite peak was not observed. This shows that the activity of the diopside was suppressed due to the presence of forsterite in the composites. Thus, the immersion time of composites was extended for another three weeks. The XRD patterns of DF1 and DF2 composites after 14 days indicated the appearance of amorphous apatite peaks (Figure 7(e,b)) whereas a small apatite peak was observed on the surface of DF3 composite after 21 days of immersion (Figure 7(h)). This difference can be explained based on the dissolution behavior discussed in earlier subsection 4.4.1.

The consumption of necessary ions from the SBF resulted in apatite deposition on the surface of DF1 and DF2 composites leading to a gradual decrease in the intensities of diopside and forsterite peaks (Figure 7(c,f). An increase in immersion time has resulted in the growth of hydroxyapatite on the surface of DF1 and DF2 samples. The high forsterite content in the DF3 composite led to slower apatite deposition. Thus, the immersion period of the DF3 composite was extended up to four weeks. The surface of the DF3 composite after 28 days showed the presence of a distinct apatite peak followed by diopside,

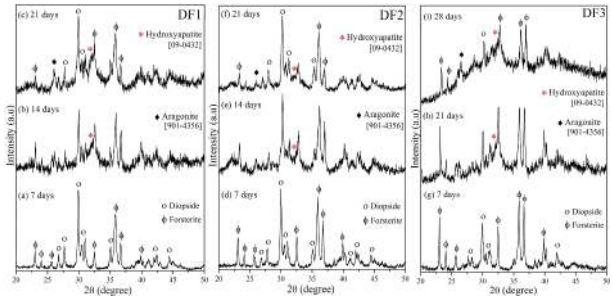

Figure 7. XRD patterns of Diopside/Forsterite Composites after Immersion in SBF.

aragonite and forsterite phases (Figure 7(i)). This study indicates that the composite comprising a higher amount of forsterite has delayed the apatite precipitation.

The diffraction peaks of hydroxyapatite observed in XRD patterns of DF1, DF2 and DF3 after immersion studies matched with standard hydroxyapatite pattern (JCPDS data card no. 09–0432). Composites with higher diopside content showed apatite layer formation on its surface within 14 days. When the diopside content was reduced to 25%, the apatite formation was delayed and noticed after 21 days. Increasing the forsterite concentration in the composites leads to a decrease in apatite deposition as the leached out Mg^{2+} ion hinders the HAp deposition.

Sadeghzade et al. (2017) prepared diopside/forsterite composites in different ratios to study their bioactivity in SBF for 21 days [17]. It was observed that the apatite deposition got enhanced as the diopside percentage was increased in the composite. Zhang et al. (2011) compared the apatite deposition ability of hydroxyapatite/diopside (90:10) composites with pure hydroxyapatite and confirmed better HAp deposition on the surface of composites in 9 days [15]. Later, Zhang et al. (2010) reported that the apatite deposited on the surface of alumina/diopside (80:20) composite within 9 days [16]. It was also noticed that the bioactivity of the composite was improved with the increase in diopside content.

Ni et al. (2008) investigated the relationship between the composition and bioactivity of wollastonite/forsterite composites [37]. A significant improvement in the apatite deposition and osteoblast proliferation was observed as the content of wollastonite in the composites was increased. The bioactivity of the forsterite was improved by preparing its composites with nano 58S bioactive glasses [39]. It was observed that no apatite was formed on the surface of pure forsterite after 21 days in SBF. Thus, the incorporation of nano 58S bioactive glass (5, 10, 20, 30 and 40 wt. %) in the forsterite matrix enhanced the rate of apatite precipitation on its surface. The release of calcium, phosphorus and silicon ions from the bioactive glass was reported to impart bioactivity to the composites. These findings show that chemical constituents,

compositional ratio and dissolution rate have influenced the biomineralization activity of diopside/forsterite composites.

4.4.4. Surface morphology and elemental analysis of deposited apatite

The difference in the rate of apatite deposition on the surface of diopside/forsterite composites has also influenced their surface morphology. Figure 8(a) shows a fibrous film covering the entire surface of DF1 composite at 28 days after the soaking into SBF. When the surface was viewed under higher magnification, the nanostructured fibrous network was noticed. These fibers were interconnected with each other and spread uniformly over the surface (Figure 8(b,c). The elemental composition of the immersed surface was characterized by EDX spectroscopy. It was found that the surface of the DF1 composite contained phosphorus accompanied by calcium, magnesium, silicon, and oxygen (Figure 8(d) which confirmed the deposition of hydroxyapatite.

DF2 composite at 28 days after the soaking into SBF (Figure 9(a,c) reveals that apatite particles were precipitated on the immersed surface and the dimensions of these particles were in the nano to micron range. As the magnification of DF2 was enhanced, some micro cracks and few pores were observed on the surface (Figure 9(b)). This may be due to the drying of the sample in a hot air oven, prior to the analysis. The DF2 composite shows phosphorus peak along with the presence of Ca, Mg, O and Si in EDX spectra (Figure 9(d)). This observation confirms that the apatite deposition took place on the surface of DF2 composite when immersed in SBF.

SEM micrographs (Figure 10(a-c)) of DF3 composite at 28 days after the soaking into SBF show apatite deposition on its surface with globular morphology.

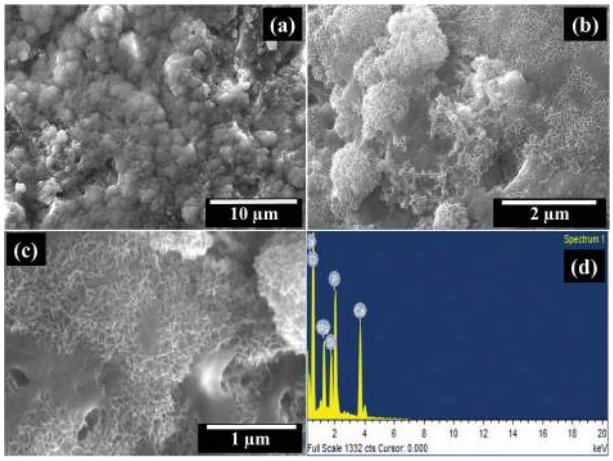

Figure 8. SEM/EDX micrographs of DF1 Composite at 28 days after the soaking into SBF. Before SEM characterization, the DF1 scaffold was dried and mounted on the stubs with adhesive carbon tapes. The DF1 composite was coated with gold in a sputter coater and analyzed under a high vacuum at 10 kV.

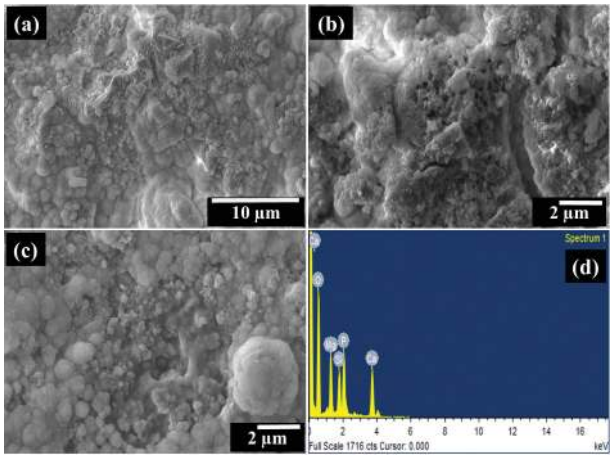

Figure 9. SEM/EDX micrographs of DF2 Composite at 28 days after the soaking into SBF. Before SEM characterization, the DF2 scaffold was dried and mounted on the stubs with adhesive carbon tapes. The DF2 composite was coated with gold in a sputter coater and analyzed under a high vacuum at 10 kV.

The presence of phosphate along with calcium, magnesium, silicon and oxygen in EDX spectra confirms apatite formation on the surface of DF3 composite (Figure 10(d)).

4.5. Degradation evaluation of composites after immersion in SBF

The degradation behavior of diopside/forsterite composites was studied by immersing it in the SBF solution for one month. The weight loss from the composites was different from each other. The composite containing more amount of diopside shows the highest weight loss and the composite containing more forsterite shows a lesser degradation rate. Thus, the highest weight loss was noticed in DF1 (0.4%) while DF3

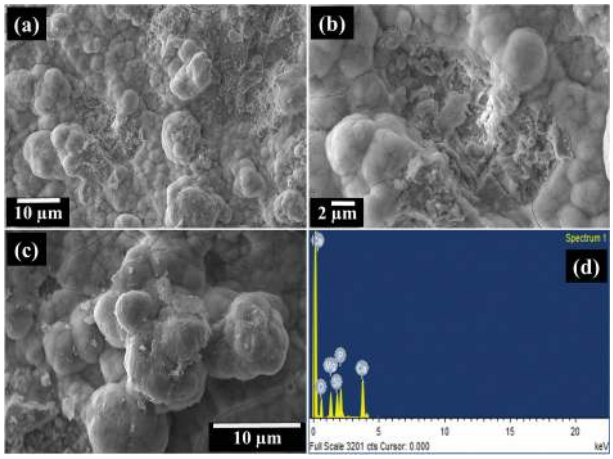

Figure 10. SEM/EDX micrographs of DF3 Composite at 28 days after the soaking into SBF. Before SEM characterization, the DF3 scaffold was dried and mounted on the stubs with adhesive carbon tapes. The DF3 composite was coated with gold in a sputter coater and analyzed under a high vacuum at 10 kV.

showed a low degradation rate (0.1%) and a slight change in the weight of DF2 composite (0.3%) was observed. The Ca-O bond has lower interatomic bonding energy than Mg-O, as a result, the availability of calcium ions in the matrix could assist in improving the degradation rate of bioceramics [40].

Sadeghzade et al. (2017) reported the degradation trend for diopside/forsterite composites in PBS solution [17]. But in current work, the SBF solution was used as an immersion medium that resulted in a very slow degradation rate. Hence, the degradation behavior of a material also depends upon the immersion medium.

4.6. Mechanical testing of composites after immersion in SBF

The mechanical stability of diopside/forsterite composites was examined after degradation study. The diopside/forsterite composites show an increase in mechanical properties with an increase in forsterite content. The average compressive load under which these composites experienced failure point were expressed in Table 4. These values indicate the change in their mechanical strength with respect to the change in composition.

DF3 composite shows a compressive strength of 154 MPa and Young's modulus of 5.56 GPa. This was found to be 1.5 times greater than DF1 composite. The compressive strength and Young's modulus of DF2 composite was found to be 122 MPa and 4.95 GPa, respectively. Among all composites, DF1 was observed to have the least mechanical strength of 102 MPa (compressive strength) and 4.13 GPa (Young's modulus). The reason for the change in strength may be due to the variation in forsterite content and the degradation behavior of the composites. The degradation rate got decreased with an increase in forsterite content. As a result, the composites become mechanically stable.

The compressive strength and Young's modulus of diopside/forsterite composite was found to be 4.36 ± 0.3 MPa and 3.08 ± 7 GPa respectively [17]. Moreover, 3D printed diopside/10% Mg-substituted wollastonite composite has a compressive strength of 37 MPa [41]. The results obtained in this work show good mechanical properties of diopside/forsterite composites after immersion in SBF for 30 days. These observations indicate that the mechanical properties of bioceramics can be increased by preparing its composites with forsterite.

Table 4. Maximum compressive load required to achieve failure point of diopside/forsterite composites.

S. No	Sample Code	Maximum Compressive Load (kN)
1	DF1	13.54
2	DF2	16.28
3	DF3	20.20

The mechanical behavior of diopside/forsterite composites was further compared with the mechanical properties of cortical bone. Table 5 shows compressive strength and Young's modulus values of cortical bone [42]. It was observed that DF3 composites possess compressive strength and Young's modulus comparable to that of cortical bone. DF2 lies near the lower limit of compressive strength and Young's modulus of cortical bone. The DF1 scaffolds have compressive strength lower than the cortical bone. Thus the mechanical properties (Young's modulus and compressive strength) of the composites were found to be altered with the variation in the forsterite content. This analysis also shows that these composites will eliminate stress shielding (osteopenia) behavior as well as provide sufficient structural support to the regenerating tissues during degradation and remodeling.

4.7. Antibacterial study of composites

The result obtained after following the well diffusion technique did not show a proper recognizable zone of inhibition on the agar plates (as shown in Figure 11). The composites showed effective results against the clinical pathogens as confirmed by broth dilution technique (Figure 12). DF1 showed the highest activity against *Staphylococcus aureus* (*S. aureus*) followed by *Escherichia coli* (*E. coli*). The inhibition pattern of the composites DF1 shows that it is effective against all the pathogens irrespective of Gram-positive or Gram-negative. However, 59.5% of *Klebsiella pneumoniae* growth was inhibited which was found to be marginal when compared to the other bacterial inhibition rate. This could be due to the presence of type 1 and type 3 fimbriae in *Klebsiella pneumoniae* that enhances the biofilm formation of the bacteria and thus results in the formation of a strong matrix of cells [43]. The breaking of the matrix of cells is challenging for the antibacterial agents which might be considered as a reason for the less inhibition of *Klebsiella pneumoniae* by DF1. DF2 inhibited the growth of *E. coli* with 66.2% followed by *S. aureus* with 63.5%. The release of calcium ions in the broth causes depolarization of the cell membrane and results in the death of bacterial cells. Thus, the presence of calcium in the composite is considered as an important factor for the antibacterial

Table 5. Comparative study between mechanical properties of bone (Data from [42]) and diopside/forsterite composites.

		Mechanical Properties	
Samples		Compressive strength (MPa)	Young's modulus (GPa)
Cortical Bone		130–200	7–30
Diopside/Forsterite Composites	DF1	92.3 ± 4.1	4.13 ± 0.3
	DF2	140.9 ± 11.2	4.95 ± 0.04
	DF3	156.7 ± 5.8	5.56 ± 0.4

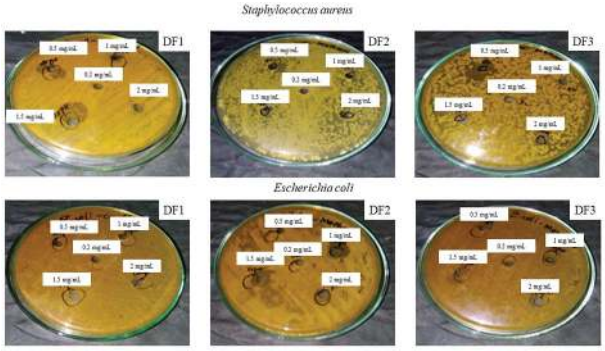

Figure 11. Well diffusion technique of antibacterial activity of the diopside/forsterite composites.

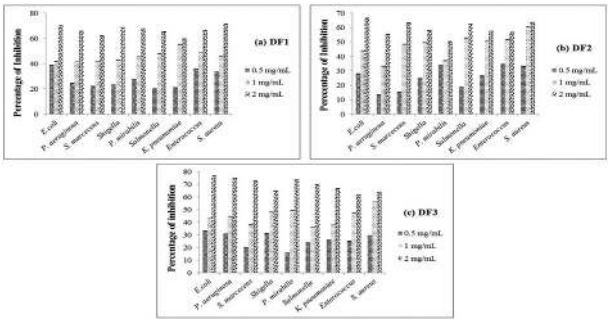

Figure 12. Percentage inhibition of different clinical pathogens by diopside/forsterite composites using broth dilution technique.

activity. The EDS analysis confirmed that the presence of calcium in the composites DF1, DF2, and DF3 was 16.29, 6.39, and 3.85 weight percent respectively. Thus, when 2 mg of DF1, DF2, and DF3 was added in the medium, approximately 0.32 mg, 0.13 mg, and 0.08 mg of calcium ions respectively were exposed to the bacterial isolates. The excess calcium ions in the cells might show cytotoxic activity in the cells or can cause apoptosis of the cells [44]. However, the observed pattern was varied in the case of DF3 composite. DF3 was highly efficient against Gram-negative bacteria (*E. coli*) isolates when compared to the Gram-positive microbes (*S. aureus*). This could be due to cellular composition and the difference in cell wall composition. The Gram-negative bacteria contain comparatively thin peptidoglycan layer bounded by outer phospholipid membrane [45].

Among all the isolates, *Enterococcus* sp. showed the lowest resistance against DF3 with 61.73% inhibition rate. The enterococcal surface protein and aggregation substance present in *Enterococcus* sp. might have aided in sustaining the virulence activity of the bacterial cells. The surface protein which is encoded by gene *esp* has been reported to enhance the formation of biofilm in *Enterococcus* sp [46]. The formation of biofilm in *Enterococcus* sp. could be considered as a reason for less inhibition of growth by DF3.

Table 6. Inhibition activity of different ceramic samples against *S. aureus* and *E. coli*.

	Bacterial Strains	
Samples	*S. aureus* Inhibition (%)	*E. coli* Inhibition (%)
EDG[28]	77.12 ± 0.08	70.44 ± 0.12
FG[27]	75.56 ± 0.07	74.16 ± 0.13
DF1	71.55 ± 0.08	69.85 ± 0.12
DF2	63.57 ± 0.05	66.37 ± 0.14
DF3	63.93 ± 0.08	76.71 ± 0.07

Table 6 shows the bacterial inhibition response of forsterite (FG) [27], diopside (EDG) [28] and diopside/forsterite composites (DF1, DF2, DF3) against *S. aureus* and *E. coli*. From this data, it was understood that EDG has more potential to inhibit *S. aureus* while FG has similar activity against both *S. aureus* and *E. coli*. Therefore, an increase in diopside (EDG) content in DF1 composite has inhibited the growth of *S. aureus*. Whereas, the higher compositional ratio of forsterite in DF3 composite has inhibited the growth of *E. coli*. In the case of DF2 sample least inhibition activity was noticed amongst all formulations. The overall study concludes that chemical constituents in the different compositional ratios can alter the antibacterial activity of the composite.

The growth of bacterial isolates was affected by a mild change in pH. An increase in pH was observed in the culture medium after incubation of 24 h. The normal pH of the Luria-Bertani broth before the inoculation of bacterial cultures was maintained at 6.8. However, in most of the cases, the pH was raised to 8 after 24 h incubation with *E. coli* (Table 7). Thus the rise in pH may be considered as the reason for inhibiting the growth of the clinical pathogens. In the case of *S. aureus*, a higher increase in pH was noticed in DF2 and DF3 as compared to DF1 (Table 8). This might be due to the difference in the dissolution rate of Ca^{2+} and Mg^{2+} ions in the culture medium. The higher pH results in the denaturation of the proteins and several cytoplasmic contents of the cells further precipitate in the medium. Once the cytoplasmic membranes are

Table 7. Changes in pH of Agar Medium after 24 h Incubation for *E. coli*.

Composites	Control	0.5 mg/mL	1 mg/mL	2 mg/mL
DF1	6.8	7.3	7.5	7.9
DF2	6.8	7.6	7.8	8
DF3	6.8	7.4	7.7	7.9

Table 8. Changes in pH of Agar Medium after 24 h Incubation for *S. aureus*.

Composites	Control	0.5 mg/mL	1 mg/mL	2 mg/mL
DF1	6.8	7.1	7.4	7.7
DF2	6.8	7.3	7.6	7.9
DF3	6.8	7.3	7.6	7.8

ruptured, the DNA is released resulting in the death of bacterial cell [47]. The calcium and magnesium ions are released in the broth during the incubation period which in turn increases the pH and deactivates the cellular mechanism of the bacterial cells [48].

The growth of *S. aureus* and *E. coli* on Mueller Hinton agar medium was compared between control and composite samples to examine the colony formation (Figure 13). Clear and distinguishable prevention in bacterial growth confirms that composites have the potential to inhibit microbial colony formation. The growth of bacterial colonies in agar medium concluded that DF1 shows similar inhibition behavior against both *S. aureus* and *E. coli* (Figure 13(b,f) while DF3 composite has the ability to inhibit the growth of *E. coli* (Figure 13(h)) more than that of *S. aureus* (Figure 13(d)).

Apart from the activity of pH, another mechanism of bacterial cell death might be a clustering of the composites around the bacteria. The bacteria are around 1–3 µm in length. Thus, the particles could easily agglomerate around the bacteria and inhibit the actions of membrane proteins to deactivate the bacterial membranes resulting in cell death by leakage of genetic materials, proteins and minerals [49]. Agglomeration of the composites around the bacterial strain was examined under scanning electron microscopy (Figure 14). The control images of *E. coli* and *S. aureus* showed smooth-surfaced cells; however, once treated with the samples, the cells were covered with layers of the composite particles.

4.8. Cell viability studies of pure samples and their composites

MTS assay is the most common test performed to analyze the viability of cells. It assists in determining the cell health, optimization of culture/experimental conditions (concentration) and measuring the survival

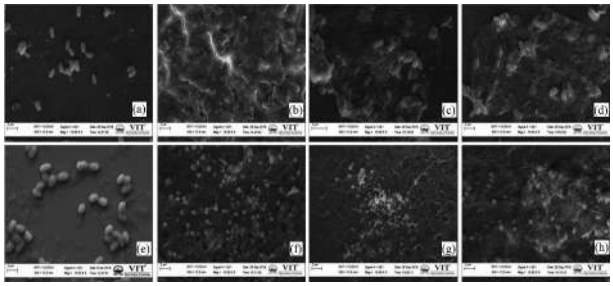

Figure 14. SEM Micrographs of Control *E. coli* (a) and after antibacterial studies with DF1- *E. coli* (b), DF2- *E. coli* (c), DF3- *E. coli* (d), Control *S. aureus* (e), agglomeration around *S. aureus* of DF1 (f), DF2 (g) and DF3 (h).

of cells in contact with samples. In the current study, MG-63 cell culture was utilized to quantify the cell viability behavior of the bioceramic samples and their composites. Figure 15 shows the viability of MG-63

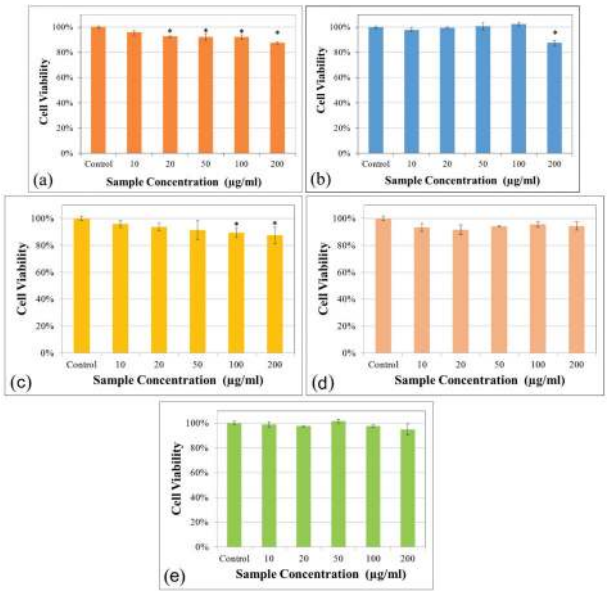

Figure 15. Viability of MG-63 Cells with (a) Pure Diopside, (b) Pure Forsterite, (c) DF1, (d) DF2, (e) DF3 after 48 h. Significant difference at * $p < 0.05$.

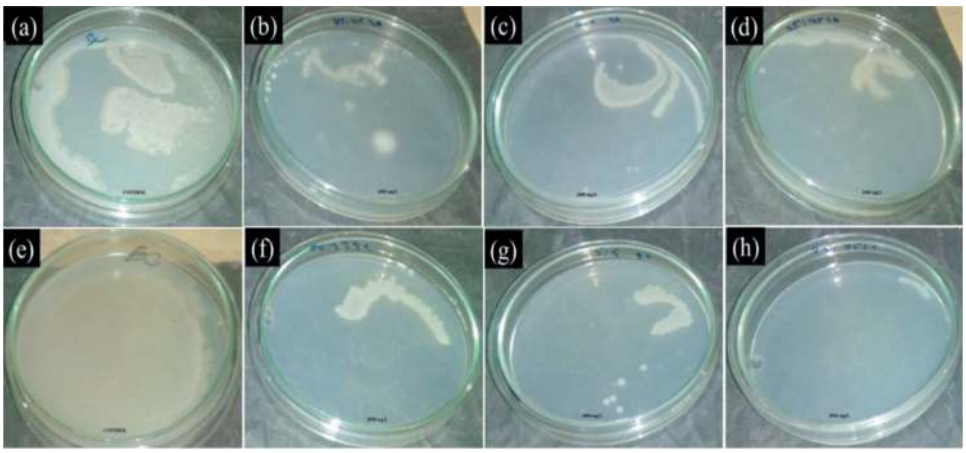

Figure 13. The growth of *S. aureus* on (a) Control, (b) DF1, (c) DF2 and (d) DF3 at 2 mg/mL in Agar Medium; The Growth of *E. Coli* on (e) Control, (f) DF1, (g) DF2 and (h) DF3 at 2 mg/mL in Agar Medium.

Cells with pure diopside and Forsterite after 48 h of incubation. It was found that an increase in the concentration of diopside in the cell culture leads to a decrease in the percentage of cell viability (Figure 15(a)). Whereas in the case of forsterite a distinct cellular behavior was noticed with respect to diopside (Figure 15(b)). Thus, forsterite possesses better viability of MG-63 cells than control as well as diopside at a concentration of 100 µg/mL.

An increase in the viability of MG-63 cells was noticed as the concentration of forsterite was increased in the composites (Figure 15(c-e)). The composites containing more amount of forsterite exhibited excellent cell viability. Thus a content-dependent effect of forsterite was observed on the viability of MG-63 cells. This observation supports the results found in the cell viability behavior of pure bioceramic samples (Figure 15(a,b)). The overall MTS assay revealed that all the tested samples (diopside, forsterite and their composites) have shown the viability of MG-63 cells higher than 85%. The trend noticed during the cell viability study of composites was DF3> DF2> DF1.

The variation in cell viability among the samples was due to the change in their chemical composition as well as the higher amount of magnesium (2 M) present in forsterite. It has been found that magnesium ion plays a key role in bone growth its repair and remodeling process [50]. Abed et al. (2009) reported that an increase in the concentration of intracellular magnesium ion can induce the proliferation of MG-63 cells [51]. Additionally, He et al. (2016) studied the influence of magnesium ion on human osteoblast activity and found that higher concentration revealed more effects on osteoblast viability [52]. Thus an increase in the number of viable cells with exposure time reveals cell proliferation ability of samples [17]. These observations indicate the cytocompatibility of pure as well as composites samples.

5. Conclusion

This study investigates the influence of forsterite incorporation on the biological and mechanical properties of diopside. The conclusions drawn from this report are: The composites showed content-dependent response toward biomineralization, degradation, mechanical stability, antibacterial activity and cytocompatibility. An increase in forsterite content enhanced the mechanical properties, cell viability whereas an increase in diopside content improves the biomineralization ability of the composites. Thus, the biocompatibility and mechanical stability of calcium-containing bioceramics can be improved by fabricating composites with magnesium silicates. The dissolution of alkaline earth ions and changes in pH were found to be the major reasons for the antibacterial activity of composites. The DF1 composite was found to be more effective toward inhibiting the growth of *S. aureus* (71.55 ± 0.08) whereas the DF3 sample revealed growth inhibition of *E. coli* inhibition up to 76.71 ± 0.07. The viability of MG-63 cells was found to be higher than 85% for all the tested samples. The trend noticed during the cell viability study of composites was DF3> DF2> DF1. The mechanical stability of the composite scaffolds was close to the lower limit of cortical bone. Amongst all formulations, the composites containing an equal compositional ratio of forsterite and diopside revealed good bioactivity, degradability, antibacterial activity as well as appropriate mechanical strength. The current report suggests that an appropriate control over the compositional ratio of chemical constituents can assist in fabricating a suitable composite material for biomedical applications.

Acknowledgments

Authors thank DST-FIST for the XRD, SEM/EDX characterization facility and SAIF/IIT-Madras for ICP-OES characterization. The authors gratefully acknowledge the financial support of the Ministry of Science and Higher Education of the Russian Federation in the framework of Increase Competitiveness Program of NUST «MISiS» (№ K4-2019-018), Moscow, Russia, implemented by a governmental decree dated 16th of March 2013, N 211.

Disclosure statement

The authors do not have any conflicts of interest to declare.

Funding

This work was supported by the Ministry of Science and Higher Education of the Russian Federation in the framework of Increase Competitiveness Program of NUST «MISiS» (№ K4-2019-018), implemented by a governmental decree dated 16th of March 2013, N 211.

ORCID

Ankita Chatterjee http://orcid.org/0000-0002-0659-5469
Marina Knyazeva http://orcid.org/0000-0002-6873-8277

References

[1] Shegarfi H, Reikeras O. Review article: bone transplantation and immune response. J Orthop Surg. 2009;17:206–211.
[2] Pedde RD, Mirani B, Navaei A, et al. Emerging biofabrication strategies for engineering complex tissue constructs. Adv Mater. 2017;29:1606061.
[3] Gomes ME, Rodrigues MT, Domingues RMA, et al. Tissue engineering and regenerative medicine: new trends and directions—a year in review. Tissue Eng Part B Rev. 2017;23:211–224.

[4] Chung U, Itaka K, Nishiyama N, et al. Scaffolds for skeletal regeneration. Nanobiotechnol. 2007;3:104–106.
[5] Roseti L, Parisi V, Petretta M, et al. Scaffolds for bone tissue engineering: state of the art and new perspectives. Mater Sci Eng C. 2017;78:1246–1262.
[6] Atala A, Kasper FK, Mikos AG. Engineering complex tissues. Sci Transl Med. 2012;4:160rv12.
[7] Saravanan C, Sasikumar S. Bioactive diopside ($CaMgSi_2O_6$) as a drug delivery carrier – a review. Curr Drug Deliv. 2012;9:583–587.
[8] Vadgama P. Surface and interface for biomaterials. Woodhead publishing limited, Cambridge: CRC Press; 2005.
[9] Wang M. Developing bioactive composite materials for tissue replacement. Biomaterials. 2003;24:2133–2151.
[10] Diba M, Goudouri O-M, Tapia F, et al. Magnesium-containing bioactive polycrystalline silicate-based ceramics and glass-ceramics for biomedical applications. Curr Opin Solid State Mater Sci. 2014;18:147–167.
[11] Kobayashi K, Okada K, Kuroda T, et al. Osteogenic cell cytotoxicity and biomechanical strength of the new ceramic Diopside. J Biomed Mater Res Part A. 1997;37:100–107.
[12] Nonami T. Developmental study of diopside for use as implant material. Mater Res Soc Proc. 1991;252:87–92.
[13] Najafinezhad A, Abdellahi M, Ghayour H, et al. A comparative study on the synthesis mechanism, bioactivity and mechanical properties of three silicate bioceramics. Mater Sci Eng C. 2017;72:259–267.
[14] Chen C, Watkins-Curry P, Smoak M, et al. Targeting calcium magnesium silicates for polycaprolactone/ceramic composite scaffolds. ACS Biomater Sci Eng. 2015;1:94–102.
[15] Zhang M, Liu C, Sun J, et al. Hydroxyapatite/diopside ceramic composites and their behaviour in simulated body fluid. Ceram Int. 2011;37:2025–2029.
[16] Zhang M, Liu C, Zhang X, et al. Al_2O_3/diopside ceramic composites and their behavior in simulated body fluid. Ceram Int. 2010;36:2505–2509.
[17] Sadeghzade S, Emadi R, Tavangarian F, et al. Fabrication and evaluation of silica-based ceramic scaffolds for hard tissue engineering applications. Mater Sci Eng C. 2017;71:431–438.
[18] Yazdanpanah A, Kamalian R, Moztarzadeh F, et al. Enhancement of fracture toughness in bioactive glass-based nanocomposites with nanocrystalline forsterite as advanced biomaterials for bone tissue engineering applications. Ceram Int. 2012;38:5007–5014.
[19] Sebdani MM, Fathi MH. Preparation and characterization of hydroxyapatite–forsterite–bioactive glass nanocomposite coatings for biomedical applications. Ceram Int. 2012;38:1325–1330.
[20] Alam F, Balani K. Adhesion force of staphylococcus aureus on various biomaterial surfaces. J Mech Behav Biomed Mater. 2017;65:872–880.
[21] Lepparanta O, Vaahtio M, Peltola T, et al. Antibacterial effect of bioactive glasses on clinically important anaerobic bacteria in vitro. J Mater Sci Mater Med. 2008;19:547–551.
[22] Hu S, Chang J, Liu M, et al. Study on antibacterial effect of 45S5 bioactive glass. J Mater SciMater Med. 2009;20:281–286.
[23] Mortazavi V, Nahrkhalaji MM, Fathi MH, et al. Antibacterial effects of sol-gel derived bioactive glass nanoparticle on aerobic bacteria. J Biomed Mater Res Part A. 2010;94:160–168.
[24] Stanic V, Dimitrijevic S, Antic-Stankovic J, et al. Synthesis, characterization and antimicrobial activity of copper and zinc-doped hydroxyapatite nanopowders. Appl Surf Sci. 2010;256:6083–6089.
[25] El-Kady AM, Ali AF, Rizk RA, et al. Synthesis, characterization and microbiological response of silver doped bioactive glass nanoparticles. Ceram Int. 2012;38:177–188.
[26] Saqaei M, Fathi M, Edris H, et al. Effects of adding forsterite bioceramic on in vitro activity and antibacterial properties of bioactive glass-forsterite nanocomposite powders. Adv Powder Technol. 2016;27:1922–1932.
[27] Choudhary R, Venkatraman SK, Chatterjee A, et al. Antibacterial forsterite (Mg_2SiO_4) scaffold: a promising bioceramic for load bearing applications. Bioact Mater. 2018;3:218–224.
[28] Choudhary R, Venkatraman SK, Chatterjee A, et al. Biomineralization, antibacterial activity and mechanical properties of biowaste derived diopside nanopowders. Adv Powder Technol. 2019;30:1950–1964.
[29] Coraça-Huber DC, Fille M, Hausdorfer J, et al. Efficacy of antibacterial bioactive glass S53P4 against S. aureus biofilms grown on titanium discs in vitro. J Orthop Res. 2014;32:175–177.
[30] Kokubo T, Takadama H. How useful is SBF in predicting in vivo bone bioactivity? Biomaterials. 2006;27:2907–2915.
[31] Esteban-Tejeda L, Prado C, Cabal B, et al. Antibacterial and antifungal activity of ZnO containing glasses. Plos One. 2015;10:e0136490.
[32] Valgas C, Souza SM, Smania EF, et al. Screening methods to determine antibacterial activity of natural products. Braz J Microbiol. 2007;38:369–380.
[33] Chatterjee A, Abraham J. Mycoremediation of 17 β-estradiol using *Trichoderma citrinoviride* strain AJAC3 along with enzyme studies. Environ Prog Sustain Energy. 2019;38:13142.
[34] Murtey MD, Ramasamy P. Sample preparations for scanning electron microscopy-life sciences. Modern electron microscopy in physical and life sciences. Croatia: IntechOpen; 2016.
[35] Kim H–M, Himeno T, Kokubo T, et al. Process and kinetics of bonelike apatite formation on sintered hydroxyapatite in a simulated body fluid. Biomaterials. 2005;26:4366–4373.
[36] Vallet-Regi M, Salinas AJ, Roman J, et al. Effect of magnesium content on the in vitro bioactivity of CaO-MgO-SiO_2-P_2O_5 sol-gel glasses. J Mater Chem. 1999;9:515–518.
[37] Ni S, Chang J, Chou L. In vitro studies of novel CaO–SiO_2–MgO system composite bioceramics. J Mater SciMater Med. 2008;19:359–367.
[38] Bueno EM, Glowacki J. Cell-free and cell-based approaches for bone regeneration. Nat Rev Rheumatol. 2009;5:685–697.
[39] Deng J, Li P, Gao C, et al. Bioactivity improvement of forsterite-based scaffolds with nano-58S bioactive glass. Mater Manuf Process. 2014;29:877–884.
[40] Callister WD, Rethwisch DG. Fundamentals of materials science and engineering. New York: John Wiley & Sons; 2008.

[41] He D, Zhuang C, Xu S, et al. 3D printing of Mg-substituted wollastonite reinforcing diopside porous bioceramics with enhanced mechanical and biological performances. Bioact Mater. 2016;1:85–92.
[42] Gerhardt L-C, Boccaccini AR. Bioactive glass and glass-ceramic scaffolds for bone tissue engineering. Materials. 2010;3:3867–3910.
[43] Schroll C, Barken KB, Krogfelt KA, et al. Role of type 1 and type 3 fimbriae in Klebsiella pneumoniae biofilm formation. BMC Microbiol. 2010;23:79.
[44] Cabal B, Alou L, Cafini F, et al. A new biocompatible and antibacterial phosphate free glass-ceramic for medical applications. Sci Rep. 2014;4:1–9.
[45] Amato E, Diaz-Fernandez YA, Taglietti A, et al. Synthesis, characterization and antibacterial activity against gram positive and gram negative bacteria of biomimetically coated silver nanoparticles. Langmuir. 2011;27:9165–9173.
[46] Tendolkar PM, Baghdayan AS, Gilmore MS, et al. Enterococcal surface protein, Esp, enhances biofilm formation by enterococcus faecalis. Infect Immun. 2004;72:6032–6039.
[47] Kumar BS, Khachatourians GG, Korber DR. High pH during trisodium phosphate treatment causes membrane damage and destruction of Salmonella enterica serovar enteritidis. Appl Environ Microbiol. 2003;69:122–129.
[48] Hu S, Ning C, Zhou Y. Antibacterial activity of silicate bioceramics. J Wuhan Univ Technol - Mater Sci Ed. 2011;26:226–230.
[49] Li Q, Mahendra S, Lyon DY, et al. Antimicrobial nanomaterials for water disinfection and microbial control: potential applications and implications. Water Res. 2008;42:4591–4602.
[50] Vormann J. Magnesium: nutrition and metabolism. Mol Aspects Med. 2003;24:27–37.
[51] Abed E, Moreau R. Importance of melastatin-like transient receptor potential 7 and magnesium in the stimulation of osteoblast proliferation and migration by platelet-derived growth factor. Am J Physiol Cell Physiol. 2009;297:C360–C368.
[52] He LY, Zhang XM, Liu B, et al. Effect of magnesium ion on human osteoblast activity. Braz J Med Biol Res. 2016;49:e5257.